

Superior Cerebellar Peduncle Atrophy in Friedreich's Ataxia Correlates with Disease Symptoms

Hamed Akhlaghi · Louise Corben ·
Nellie Georgiou-Karistianis · John Bradshaw ·
Elsdon Storey · Martin B. Delatycki · Gary F. Egan

Published online: 24 November 2010
© Springer Science+Business Media, LLC 2010

Abstract Friedreich's ataxia (FRDA) is the most common early onset inherited ataxia with clinical manifestations, including gradual progression of unremitting cerebellar–sensory ataxia, peripheral sensory loss, loss of lower limb tendon reflexes and hypertrophic cardiomyopathy. Although atrophy of the superior cerebellar peduncle (SCP) has been reported in several magnetic resonance imaging (MRI) studies of FRDA, the relationship of SCP changes to genetic and clinical features of FRDA has not been investigated. We acquired T1-weighted MRI scans in 12 right-handed individuals with FRDA, homozygous for a GAA expansion in intron 1 of *FXN*, as well as 13 healthy age-matched controls. The corrected cross-sectional areas of the right (left) SCP in the individuals with FRDA (R, $20 \pm 7.9 \text{ mm}^2$; L, $25 \pm 5.6 \text{ mm}^2$) were significantly smaller than for controls (R, $68 \pm 16 \text{ mm}^2$; L, $78 \pm 17 \text{ mm}^2$) ($p < 0.001$). The SCP volumes of individuals with FRDA were negatively correlated with Friedreich's ataxia rating scale score ($r = -0.553$) and

disease duration ($r = -0.541$), and positively correlated with the age of onset ($r = 0.548$) ($p < 0.05$). These findings suggest that structural MR imaging of the SCP can provide a surrogate marker of disease severity in FRDA and support the potential role of structural MRI as a biomarker in the evaluation of neurodegenerative diseases and therapies.

Keywords Friedreich's ataxia · Superior cerebellar peduncle · Cerebellum · Volumetric MRI

Introduction

Friedreich's ataxia (FRDA) is the most common early onset inherited ataxia with a prevalence of around 2×10^{-5} in Caucasians [1]. The clinical manifestations of the disease are gradual progression of unremitting cerebellar–sensory ataxia, peripheral sensory loss, loss of lower limb tendon

H. Akhlaghi (✉) · G. F. Egan
Florey Neurosciences Institute, Centre for Neurosciences,
University of Melbourne,
Parkville, VIC, Australia
e-mail: h.akhlaghi@pgrad.unimelb.edu.au

G. F. Egan
e-mail: gary.egan@florey.edu.au

L. Corben · M. B. Delatycki
Bruce Lefroy Centre for Genetic Health Research,
Murdoch Childrens Research Institute,
Parkville, VIC, Australia

L. Corben
e-mail: louise.corben@ghsv.org.au

M. B. Delatycki
e-mail: martin.delatycki@ghsv.org.au

L. Corben · N. Georgiou-Karistianis · J. Bradshaw
Experimental Neuropsychology Research Unit,
School of Psychology and Psychiatry, Monash University,
Clayton, VIC, Australia

N. Georgiou-Karistianis
e-mail: nellie.georgiou-karistianis@med.monash.edu.au

J. Bradshaw
e-mail: j.l.bradshaw@med.monash.edu.au

E. Storey
Department of Medicine (Neurosciences),
Monash University (Alfred Hospital Campus),
Prahran, VIC, Australia
e-mail: elsdon.storey@med.monash.edu.au

M. B. Delatycki
Department of Clinical Genetics, Austin Health,
Heidelberg, VIC, Australia

reflexes, scoliosis and hypertrophic cardiomyopathy [1]. In 98% of affected individuals, FRDA is due to homozygous expansions of a GAA trinucleotide repeat in intron 1 of the *FXN* gene [2]. The underlying neuropathology of FRDA is loss of large primary neurons in the dorsal root ganglia, loss of sensory fibres in the peripheral nerves, degeneration of the posterior columns of the spinal cord and atrophy of the dentate nucleus of the cerebellum [1, 3].

Several magnetic resonance imaging (MRI) studies have demonstrated atrophy of the spinal cord in early stages of FRDA, followed by brain stem and cerebellar atrophy later in the course of the disease [4–7]. Voxel-based morphometry has illustrated volume loss in the dentate region of the cerebellum, as well as in the dorsal medulla, inferomedial areas of the cerebellar hemispheres and rostral vermis [8].

The dentate nucleus plays an important role as a relay centre between the cortex and other brain structures, via the superior cerebellar peduncle (SCP), which contains its efferent fibres [9–11]. Although atrophy of the SCP has been reported in several MRI studies in FRDA [12], the relationship of SCP changes to genetic and clinical features of FRDA has not been systemically investigated. We hypothesized that the extent of atrophy of the SCP in individuals, with genetically proven FRDA, would correlate with genetic and clinical features of FRDA, with greater atrophy observed in individuals with more severe clinical symptoms (as measured by the Friedreich's ataxia rating scale, FARS) [13] and in patients with longer disease duration. The core aim of this study was to demonstrate whether structural MRI could be adopted as a biomarker in rating the severity of FRDA. At present, there is insufficient evidence to implement volumetric assessment of white matter changes as a surrogate marker of FRDA.

Methods

Twelve right-handed individuals with FRDA, homozygous for a GAA expansion in intron 1 of *FXN*, were recruited

from the Monash Medical Centre Friedreich Ataxia Clinic, Victoria, Australia. Thirteen healthy age-matched controls with no known neurological disorders were also recruited. There was no difference between the mean age of the individuals with FRDA (34.5 ± 9 years) and controls (33 ± 7 years). FARS scores were determined by one author (MBD) within 3 months of the scanning session (Table 1).

The structural MR study was part of a larger study that included acquisition of two fMRI and DTI sequences. The full study protocol required that each patient was in the scanner for approximately 90 min, divided into two 45-min sessions. A T1-weighted structural image was acquired for each participant using the 3T Siemens MRI located at the Royal Children's Hospital, Melbourne (field of view, 224×256 mm, acquisition matrix 256×256 , repetition time/echo time/inversion time/FLIP angle = 11.8 ms/2.4 ms/900/9°). This yielded 512 contiguous 0.5-mm thick slices and 0.5×0.5 mm² in-plane resolution. The DICOM files were then transferred to a DICOM server and converted to ANALYZE format using FSL [14]. T1 images were aligned to an MNI template using a rigid body transformation algorithm (FLIRT, Oxford University, UK) [15]. Subsequently using the FMRIB's Automated Segmentation Tool (FAST) [16], the ANALYZE files were segmented into white matter, grey matter and CSF. The white matter mask created after FAST segmentation was used to section the superior cerebellar peduncle. The boundaries of the SCP were defined as follows: inferiorly by the posterior border of the pons, medially and laterally by the CSF and the fourth ventricle, and superiorly by the inferior colliculus. The lateral and medial borders of the white matter mask defined the lateral and medial limits of the SCP (CSF and fourth ventricle). The posterior and inferior borders of the SCP were demarcated by the operator. This process was performed on two occasions separated by a 2-week interval.

The SCP was sectioned from the most anterior point into 1-mm thick images (see Fig 1). After excluding the first two slices, the average cross-sectional area of the SCP was then corrected based on the total intracranial volume (TIV)

Table 1 Group characteristics

	FRDA participants	Controls	<i>P</i> value
Number (males, females)	12 (5,7)	13 (5,8)	–
Mean age, years	34.5 ± 9	33 ± 7	n/s
Total intracranial volume, cm ³	$(1.42 \pm 0.15) \times 10^3$	$(1.49 \pm 0.11) \times 10^3$	n/s
Volume of cerebellum ^a , cm ³	131 ± 15	146 ± 11	n/s
Mean disease duration, years	15 ± 6	–	–
Age of onset, years	19 ± 6	–	–
Larger GAA repeat	$1,007 \pm 107$	–	–
Smaller GAA repeat	649 ± 205	–	–
FARS score (range)	88 ± 15 (63–113)	–	–
Stroop task, seconds	49 ± 16	56 ± 7	n/s

Dashes indicate where descriptives were not applicable

n/s not significant

^aUncorrected volumes

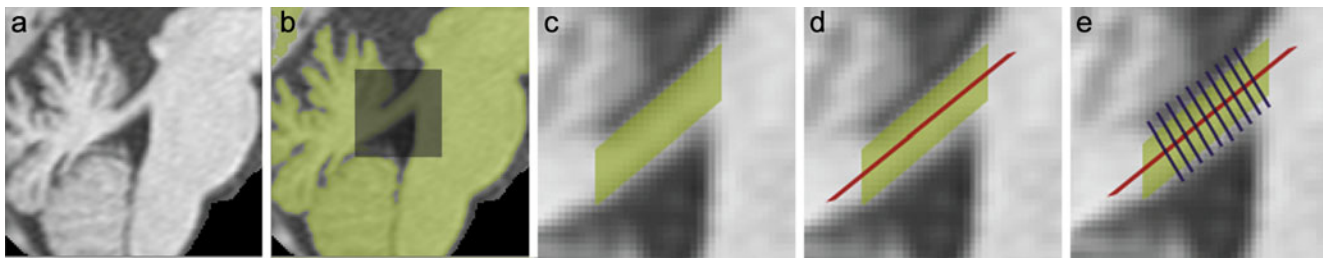


Fig. 1 Segmentation and sectioning of the superior cerebellar peduncle. **a** Sagittal T1 MRI of the posterior cranial fossa, including the superior cerebellar peduncle (SCP). **b** Segmentation of the brain tissue into the white matter, grey matter and the CSF: the *yellow area*

represents the white matter. The *black box* delineates the zoomed area in figure (c–e). **c** The segmented SCP as described in the method section. **d** The *red line* indicates the main axis of the SCP. **e** The *blue lines* illustrate the slices of the SCP at 1 mm intervals

of each participant using the following method to reduce interindividual variation:

$$SCP_{corrected} = SCP_{uncorrected} \times (TIV_{mean}/TIV_{participant}) \quad (1)$$

where TIV_{mean} is the average total intracranial volume of the controls, $TIV_{participant}$ is the total intracranial volume of each participant and $SCP_{uncorrected}$ is the actual measurement of the average cross-sectional area of the SCP.

We also normalized the cross-sectional area of the SCP based on a method [2] described by Jack et al. [17]. This method improves distributional properties of volumetric values (i.e., produces a more nearly Gaussian distribution) in comparison with a ratio adjustment method which tends to positively skew them. Two volumetric studies applied this method to correct their measurements [18, 19].

$$SCP_{normalized} = SCP_{uncorrected} \times (TIV_{mean}/TIV_{participant})^{\alpha} \quad (2)$$

where α is a regression coefficient of the TIV and SCP volumes in healthy controls.

The Bland–Altman method [20, 21] was used to assess limits of agreement and estimate repeatability of the method of the SCP segmentation. Furthermore, the analysis of the SCPs was performed independently by a second observer with expertise in neuroradiology, who was blinded to the participant diagnoses, to ensure that the correct region of the brain had been segmented and analyzed. The cerebellum segmentation and volume measurement was performed using the spatially unbiased atlas template method [22, 23].

All participants were screened for symptoms of depression at the time of testing using the Beck depression inventory [24]. Participants also completed all three conditions of the Stroop Interference Test [25] to screen for impaired planning and inhibitory processes. They also completed the National Adult Reading Test [26] to establish an estimate of IQ. Changes in cognitive function in people with FRDA have been suggested [27, 28], and the Stroop task includes an internal condition to control for visual scanning and articulation deficits; meaning it is therefore suitable for use in this population.

All statistical analyses were undertaken using MATLAB version 7 (The MathWorks Inc., Natick, MA) and SPSS version 15 (SPSS Inc., Chicago, IL). To account for age-related brain atrophy in our analyses, age of participants was defined as a covariate in SPSS.

Standard protocol approvals, registrations and patient consents The study was approved by the Melbourne Health Ethics Committee and all participants consented to engage in this study.

Results

The TIV and cerebellar volume of the individuals with FRDA $[(1.42 \pm 0.15) \times 10^3 \text{ cm}^3, 131 \pm 15 \text{ cm}^3]$ did not significantly differ from controls $[(1.49 \pm 0.11) \times 10^3 \text{ cm}^3, 146 \pm 11 \text{ cm}^3]$. Figure 2 shows the 95% confidence limits of agreement between the two SCP segmentations. No significant correlation was observed between the difference between the SCP measurements and the mean SCP measurement (Spearman's rank correlation coefficient $[r_s] = -0.054, p \text{ value} > 0.05$). The Bland–Altman repeatability coefficient was 4.31 mm^2 . There was a significant positive correlation between TIV and the mean of uncorrected right and left SCP cross-sectional areas in the controls ($p = 0.027$). Based on this correlation, the α value for Eq. 2 was set to 0.549.

The corrected cross-sectional areas of the right (left) SCP in the individuals with FRDA were $20 \pm 7.9 \text{ mm}^2$ ($25 \pm 5.6 \text{ mm}^2$) and $68 \pm 15.8 \text{ mm}^2$ ($78 \pm 16.7 \text{ mm}^2$) in the controls. Repeated measures analysis was used to compare the corrected cross-sectional areas of the SCP between the groups, specifying age as a covariate factor. The corrected cross-sectional area of the SCP in the FRDA participants was significantly reduced compared with the controls ($[F(1,22) = 126.52, p < 0.001]$; see Fig 3). Although no significant differences between the right and left corrected SCP cross-sectional areas in the individuals with FRDA ($[F(1,22) = 3.417, p = 0.078]$) or in the

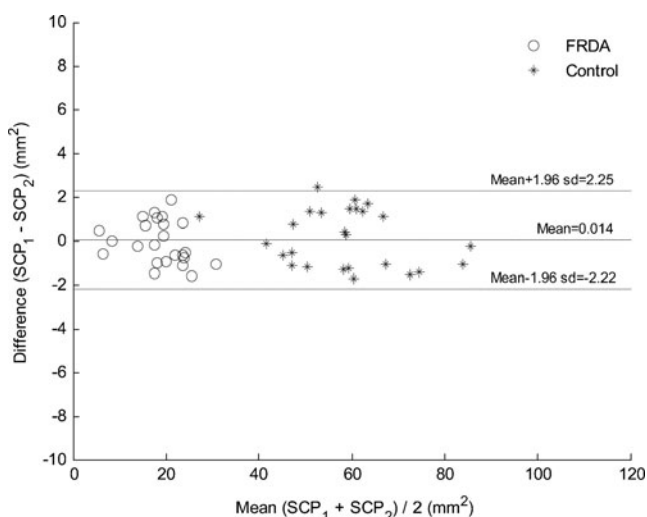


Fig. 2 Bland–Altman plot to assess agreements between the two SCP segmentation measurements. Plot of the Bland–Altman revised method for repeatability assessments showing the difference between the two SCP segmentation measurements compared to the mean segmentation results (*dashed line*). The upper and lower two standard deviation limits from the mean difference of the SCP measurements are also shown (*dotted lines*). SCP_1 , mean cross-sectional measurement of the SCP from the first segmentation; SCP_2 , mean cross-sectional measurement of the SCP from the first segmentation; *sd* standard deviation

control group [$F(1,24) = 2.44$, $p = 0.131$] were detected at the level $p < 0.05$, there was a trend for the right SCP to be smaller in both groups.

The normalized cross-sectional areas of the SCP also showed significant reduction in individuals with FRDA

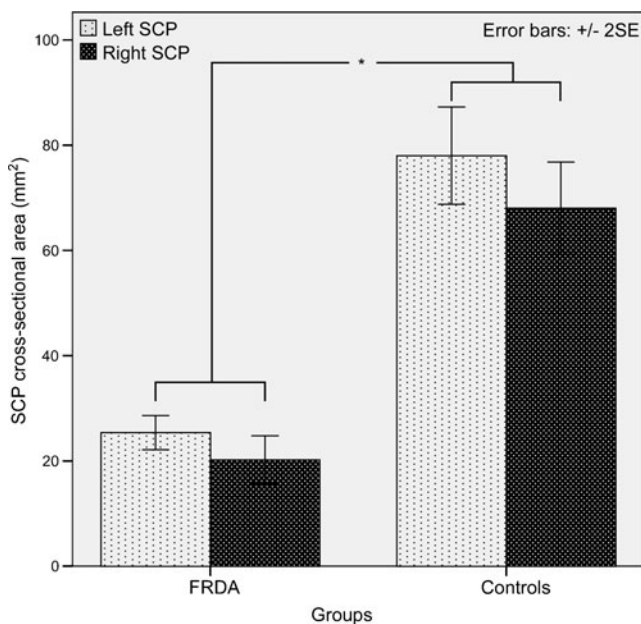


Fig. 3 Corrected superior cerebellar peduncle cross-sectional area in the individuals with FRDA and controls. Corrected superior cerebellar peduncle cross-sectional area. The cross-sectional area of the SCP is significantly smaller in individuals with FRDA compared with healthy controls ($p < 0.001$, corrected for repeated measurements)

compared with healthy controls ($[F(1,22) = 147.29$, $p < 0.001]$).

A one-tailed partial correlation test was performed between the normalized cross-sectional area of the left and right SCP in the FRDA participants and disease parameters, including age at onset; FARS score; disease duration; size of the smaller and larger GAA repeats, using age as a covariant. There was no correlation between the normalized cross-sectional area of the left and right SCP and either GAA repeat, depression score, IQ or Stroop task performance; however, the normalized SCP volumes of FRDA participants were significantly negatively correlated with the FARS score ($r = -0.553$) and disease duration ($r = -0.541$), and positively correlated with the age of onset ($r = 0.548$) ($p < 0.05$, $df = 9$ for all correlations; see Fig 4).

Discussion

We quantified the cross-sectional area of the SCP in individuals with FRDA using T1-weighted MRI and demonstrated that the cross-sectional areas of the SCP in these individuals were negatively correlated with FARS scores and disease duration, and correlated positively with the age of onset. Findings suggest that the SCP is approximately 60% smaller in FRDA subjects than in the controls and that this reduction becomes more prominent with disease progression.

The difference between the measurements of the two segmentations of the SCP lay within the 95% confidence limits of the mean of the SCP measurements, which demonstrated high repeatability of the SCP segmentation method. The mean difference between the measurements was not clinically significant.

Earlier imaging investigations in FRDA demonstrated atrophy of the upper cervical spinal cord (anteroposterior volumetric reduction), with mild cerebellar volume loss in the late stages of the disease [4, 6, 7, 29, 30]. The characteristic neuropathological changes in FRDA are degeneration of the posterior columns of the spinal cord, including the gracilis and cuneatus tracts, together with neuronal loss in the dorsal root ganglia [2, 3].

The dentate nucleus is the most severely affected region of the cerebellum in FRDA, and loss of myelinated fibres in the hilum of the dentate nucleus is prominent [31]. Ramos et al. [32] showed cerebellar atrophy and increased area of the fourth ventricle in individuals with FRDA using CT scans and suggested these changes reflect atrophy of the dentate nucleus. The dentate nucleus projections into the motor, premotor, oculomotor, prefrontal and posterior parietal cortex pass through the superior cerebellar peduncle and the thalamus [33, 34]. Increased accumulation of iron in the dentate nucleus has been demonstrated in

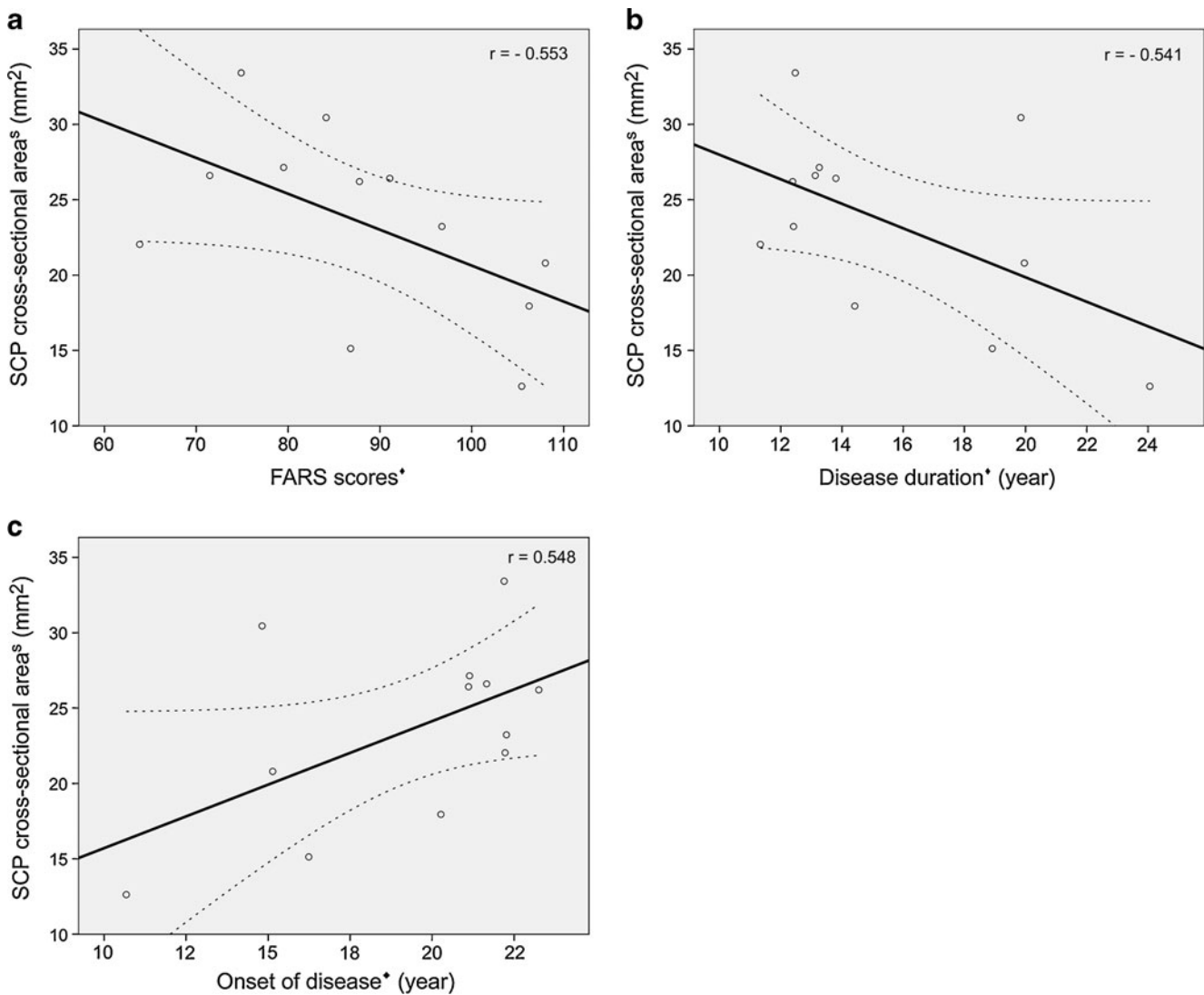


Fig. 4 Correlation graphs between normalized SCP and FARS score, disease duration and onset of disease. Partial correlation graphs between the normalized SCP cross-sectional area and (a) FARS

scores, (b) disease duration and (c) age of onset in individuals with FRDA ($p < 0.05$ for all). *Black diamond* adjusted values

FRDA, suggesting the pathogenesis of neuronal loss is at least partly due to oxidative damage [35]. A voxel-based analysis of structural images in FRDA illustrated symmetric loss of the white matter in the dentate region compared with healthy controls [8, 12]. Furthermore, a recent VBM study also demonstrated atrophy of the SCP in FRDA using a region of interest analysis in the brainstem and cerebellum and also detected subtle abnormalities in the posterior cranial fossa [36]. White matter volume in this region correlated negatively with disease severity (as measured by the International Cooperative Ataxia Rating Scale (ICARS) and the Inherited Ataxia Clinical Rating Scale) and with disease duration. Della Nave et al. and Pagani et al. [12, 37] also found decreased fractional anisotropy (FA) and increased mean diffusivity in the SCP of individuals with FRDA using an automated method, tract-based spatial

statistics [38], to investigate white matter without a priori hypotheses. Their study illustrated an inverse correlation between the decreased FA value in the left SCP and the severity of neurological deficits as assessed by ICARS score. We have shown that there is a trend for the mean cross-sectional area of the left SCP to be larger than that of the right, in both individuals with FRDA and healthy controls. This asymmetry between the left and right SCPs was also found in the recent study by Della Nave et al. [12]. Further studies with larger sample size are required to investigate asymmetric left and right SCPs in individuals with FRDA.

MRI has been widely used in the diagnosis and assessment of neurodegenerative diseases of the CNS. Recently, several studies have proposed that MRI can act as a reliable surrogate marker to assess the severity and

progression of neurodegenerative diseases [39–41]. In clinical settings, structural MRI has been extensively utilized to assess the progression of neurodegenerative diseases such as Huntington's disease (HD) and to determine the efficacy of treatments in the long run. Several studies have shown that striatal atrophy in clinical HD correlates with disease severity, total functional capacity and deficits in memory, executive function and processing speed [41]. Here, we have demonstrated that atrophy of the SCP shows a strong correlation with FRDA disease severity.

Ataxia rating scales are neurologic assessment methods designed to assess the severity and progression of patients with degenerative ataxias such as FRDA. The FARS and ICARS are commonly used in clinical trials and clinical assessments in FRDA [42]. Although these methods have good to excellent inter-rater reliability [13, 43, 44], they are somewhat subjective, potentially non-linear and are prone to clinician bias. This study illustrates that SCP atrophy in FRDA participants is negatively correlated with the FARS score. We suggest that imaging can be implemented as a sensitive and objective measurement of disease progression used in conjunction with other neurologic assessments.

While this study showed the normalized cross-sectional area of the SCP in individuals with FRDA positively correlates with the age of onset and negatively with disease duration, these findings do not imply that they are interdependent and have similar effects on disease severity and progression. Corben et al. [28] found that movement reprogramming in individuals with FRDA was negatively correlated with age of onset, not disease duration. Although, longer disease duration is associated with more severe symptoms in FRDA, they argued that earlier onset of the disease negatively impacts brain and cerebellar development. The results of the current study support this conclusion.

A limitation of this study is the small sample size. Since individuals with a FARS score over 120 would have significant difficulty getting onto the MRI scanner table and completing the MR imaging procedure, the highest FARS score in individuals with FRDA in this study was 113. Hence, individuals with higher disability were excluded from the study because of the difficulty (*and safety issues*) associated with placing a significantly impaired wheelchair-dependent patient onto the MRI table. Future studies with a larger sample size, including a broader range of disease severity could be undertaken to extend the findings of this study to the full spectrum of disease severity.

This study demonstrates that the SCP is significantly reduced in size in individuals with FRDA, and that this reduction is negatively correlated with FARS score and disease duration and positively correlated with age of onset.

These findings provide evidence to suggest that structural MR imaging of the SCP can alternatively be used to assess disease severity in FRDA and support the potential role of structural MRI as a biomarker in the evaluation of disease progression and the response to therapies for this disorder.

Acknowledgments We thank the participants for taking part in this study. This study was supported by funding from the Friedreich Ataxia Research Association (Australasia), Friedreich Ataxia Research Alliance (USA) and Murdoch Childrens Research Institute. HA received a Melbourne International fee remission scholarship and a Melbourne International Research scholarship. MBD is an NHMRC practitioner fellow. GFE is an NHMRC research fellow.

Conflict of Interest Dr. Hamed Akhlaghi received a Melbourne International Fee Remission Scholarship and a Melbourne International Research Scholarship.

Professor Elsdon Storey has received honoraria (payable to his institution) from Pfizer for lecturing on non-drug-related issues at an education course. He is a co-investigator on an NIH trial for which Merck is providing active drug (aspirin and placebo).

Professor Martin B. Delatycki is associate editor for BMC Neurology; he receives grants from NHMRC, Friedreich Ataxia Research Alliance, Friedreich Ataxia Research Association, and he is on the Pfizer Australia Neuroscience Grant Panel.

References

- Pandolfo M. Friedreich ataxia: the clinical picture. *J Neurol*. 2009;256 Suppl 1:3–8.
- Campuzano V, Montermini L, Molto MD, Pianese L, Cossee M, Cavalcanti F, et al. Friedreich's ataxia: autosomal recessive disease caused by an intronic GAA triplet repeat expansion. *Science*. 1996;271(5254):1423–7.
- Alper G, Narayanan V. Friedreich's ataxia. *Pediatr Neurol*. 2003;28(5):335–41.
- Wullner U, Klockgether T, Petersen D, Naegel T, Dichgans J. Magnetic resonance imaging in hereditary and idiopathic ataxia. *Neurology*. 1993;43(2):318–25.
- Huang YP, Tuason MY, Wu T, Plaitakis A. MRI and CT features of cerebellar degeneration. *J Formos Med Assoc*. 1993;92(6):494–508.
- Ormerod IE, Harding AE, Miller DH, Johnson G, MacManus D, du Boulay EP, et al. Magnetic resonance imaging in degenerative ataxic disorders. *J Neurol Neurosurg Psychiatry*. 1994;57(1):51–7.
- De Michele G, Di Salle F, Filla A, D'Alessio G, Ambrosio G, Viscardi L, et al. Magnetic resonance imaging in "typical" and "late onset" Friedreich's disease and early onset cerebellar ataxia with retained tendon reflexes. *Ital J Neurol Sci*. 1995;16(5):303–8.
- Della Nave R, Ginestroni A, Giannelli M, Tessa C, Salvatore E, Salvi F, et al. Brain structural damage in Friedreich's ataxia. *J Neurol Neurosurg Psychiatry*. 2008;79(1):82–5.
- Braak H, Braak E. Morphological studies of local circuit neurons in the cerebellar dentate nucleus of man. *Hum Neurobiol*. 1983;2(2):49–57.
- Yamaguchi K, Goto N. Three-dimensional structure of the human cerebellar dentate nucleus: a computerized reconstruction study. *Anat Embryol Berl*. 1997;196(4):343–8.
- Milosevic NT, Ristanovic D, Maric DL, Rajkovic K. Morphology and cell classification of large neurons in the adult human dentate nucleus: a quantitative study. *Neurosci Lett*. 2010;468(1):59–63.
- Della Nave R, Ginestroni A, Tessa C, Salvatore E, Bartolomei I, Salvi F, et al. Brain white matter tracts degeneration in Friedreich

- ataxia. An in vivo MRI study using tract-based spatial statistics and voxel-based morphometry. *NeuroImage*. 2008;40(1):19–25.
13. Subramony SH, May W, Lynch D, Gomez C, Fischbeck K, Hallett M, et al. Measuring Friedreich ataxia: interrater reliability of a neurologic rating scale. *Neurology*. 2005;64(7):1261–2.
 14. Smith SM, Jenkinson M, Woolrich MW, Beckmann CF, Behrens TE, Johansen-Berg H, et al. Advances in functional and structural MR image analysis and implementation as FSL. *Neuroimage*. 2004;23 Suppl 1:S208–19.
 15. Jenkinson M, Smith S. A global optimisation method for robust affine registration of brain images. *Med Image Anal*. 2001;5(2):143–56.
 16. Zhang Y, Brady M, Smith S. Segmentation of brain MR images through a hidden Markov random field model and the expectation-maximization algorithm. *IEEE Trans Med Imaging*. 2001;20(1):45–57.
 17. Jack CR, Twomey CK, Zinsmeister AR, Sharbrough FW, Petersen RC, Cascino GD. Anterior temporal lobes and hippocampal formations: normative volumetric measurements from MR images in young adults. *Radiology*. 1989;172(2):549–54.
 18. Barnes J, Scallan RI, Boyes RG, Frost C, Lewis EB, Rossor CL, et al. Differentiating AD from aging using semiautomated measurement of hippocampal atrophy rates. *Neuroimage*. 2004;23(2):574–81.
 19. Paviour DC, Price SL, Stevens JM, Lees AJ, Fox NC. Quantitative MRI measurement of superior cerebellar peduncle in progressive supranuclear palsy. *Neurology*. 2005;64(4):675–9.
 20. Bland JM, Altman DG. Statistical methods for assessing agreement between two methods of clinical measurement. *Lancet*. 1986;1(8476):307–10.
 21. Bland JM, Altman DG. Measuring agreement in method comparison studies. *Stat Methods Med Res*. 1999;8(2):135–60.
 22. Diedrichsen J. A spatially unbiased atlas template of the human cerebellum. *Neuroimage*. 2006;33(1):127–38.
 23. Diedrichsen J, Balsters JH, Flavell J, Cussans E, Ramnani N. A probabilistic MR atlas of the human cerebellum. *Neuroimage*. 2009;46(1):39–46.
 24. Beck AT, Ward CH, Mendelson M, Mock J, Erbaugh J. An inventory for measuring depression. *Arch Gen Psychiatry*. 1961;4:561–71.
 25. Golden CJ. The Stroop Color and Word Test. A manual for clinical and experimental uses. Chicago: Stoelting; 1978.
 26. Nelson HE, O'Connell A. Dementia: the estimation of premorbid intelligence levels using the New Adult Reading Test. *Cortex*. 1978;14(2):234–44.
 27. Corben LA, Georgiou-Karistianis N, Fahey MC, Storey E, Churchyard A, Horne M, et al. Towards an understanding of cognitive function in Friedreich ataxia. *Brain Res Bull*. 2006;70(3):197–202.
 28. Corben LA, Delatycki MB, Bradshaw JL, Horne MK, Fahey MC, Churchyard AJ, et al. Impairment in motor reprogramming in Friedreich ataxia reflecting possible cerebellar dysfunction. *J Neurol*. 2009;257(5):782–89.
 29. Wessel K, Schroth G, Diener HC, Muller-Forell W, Dichgans J. Significance of MRI-confirmed atrophy of the cranial spinal cord in Friedreich's ataxia. *Eur Arch Psychiatry Neurol Sci*. 1989;238(4):225–30.
 30. Mascalchi M, Salvi F, Piacentini S, Bartolozzi C. Friedreich's ataxia: MR findings involving the cervical portion of the spinal cord. *Am J Roentgenol*. 1994;163(1):187–91.
 31. Barbeau A. The Quebec cooperative study of Friedreich's ataxia: 1974–1984—10 years of research. *Can J Neurol Sci*. 1984;11(4 Suppl):646–60.
 32. Ramos A, Quintana F, Diez C, Leno C, Berciano J. CT findings in spinocerebellar degeneration. *Ajnr*. 1987;8(4):635–40.
 33. Middleton FA, Strick PL. Cerebellar projections to the prefrontal cortex of the primate. *J Neurosci*. 2001;21(2):700–12.
 34. Kelly RM, Strick PL. Cerebellar loops with motor cortex and prefrontal cortex of a nonhuman primate. *J Neurosci*. 2003;23(23):8432–44.
 35. Waldvogel D, van Gelderen P, Hallett M. Increased iron in the dentate nucleus of patients with Friedreich's ataxia. *Ann Neurol*. 1999;46(1):123–5.
 36. Franca Jr MC, D'Abreu A, Yasuda CL, Bonadia LC, Santos da Silva M, Nucci A, et al. A combined voxel-based morphometry and 1H-MRS study in patients with Friedreich's ataxia. *J Neurol*. 2009;256(7):1114–20.
 37. Pagani E, Gimestrioni A, Della Nave R, Agosta F, Salvi F, De Michele G, et al. Assessment of brain white matter fiber bundle atrophy in patients with Friedreich ataxia. *Radiology*. 2010;255(3):882–9.
 38. Smith SM, Jenkinson M, Johansen-Berg H, Rueckert D, Nichols TE, Mackay CE, et al. Tract-based spatial statistics: voxelwise analysis of multi-subject diffusion data. *Neuroimage*. 2006;31(4):1487–505.
 39. Pia Sormani M, Bruzzi P, Comi G, Filippi M. MRI metrics as surrogate markers for clinical relapse rate in relapsing–remitting MS patients. *Neurology*. 2002;58(3):417–21.
 40. Scheltens P, Barkhof F, Fazekas F. White matter changes on MRI as surrogate marker. *Int Psychogeriatr*. 2003;15(SupplementS1):261–5.
 41. Bohanna I, Georgiou-Karistianis N, Hannan AJ, Egan GF. Magnetic resonance imaging as an approach towards identifying neuropathological biomarkers for Huntington's disease. *Brain Res Rev*. 2008;58(1):209–25.
 42. Delatycki MB. Evaluating the progression of Friedreich ataxia and its treatment. *J Neurol*. 2009;256 Suppl 1:36–41.
 43. Storey E, Tuck K, Hester R, Hughes A, Churchyard A. Inter-rater reliability of the international cooperative ataxia rating scale (ICARS). *Mov Disord*. 2004;19(2):190–2.
 44. Lynch DR, Farmer JM, Tsou AY, Perlman S, Subramony SH, Gomez CM, et al. Measuring Friedreich ataxia: complementary features of examination and performance measures. *Neurology*. 2006;66(11):1711–16.